Electrochimica Acta 152 (2015) 496–504

Contents lists available at ScienceDirect

Electrochimica Acta

journal homepage: www.elsevier.com/locate/electacta

Study on electrochemical performance and mechanism of V-doped Li_2FeSiO_4 cathode material for Li-ion batteries

Lu-Lu Zhang [a,b], Hua-Bin Sun [a], Xue-Lin Yang [a,*], Yan-Wei Wen [c], Yun-Hui Huang [c], Ming Li [a], Gang Peng [a], Hua-Chao Tao [a], Shi-Bing Ni [a], Gan Liang [d]

[a] College of Materials and Chemical Engineering, Hubei Provincial Collaborative Innovation Center for New Energy Microgrid, China Three Gorges University, 8 Daxue Road, Yichang, Hubei 443002, China
[b] CAS Key Laboratory of Materials for Energy Conversion, Shanghai Institute of Ceramics, Chinese Academy of Sciences, Shanghai 200050, China
[c] School of Materials Science and Engineering, State Key Laboratory of Material Processing and Die & Mould Technology, Huazhong University of Science and Technology, 1037 Luoyu Road, Wuhan, Hubei 430074, China
[d] Department of Physics, Sam Houston State University, Huntsville, Texas 77341, USA

ARTICLE INFO

Article history:
Received 12 October 2014
Received in revised form 23 November 2014
Accepted 26 November 2014
Available online 27 November 2014

Keywords:
Lithium ion battery
Cathode
Lithium iron orthosilicate
Vanadium-doping

ABSTRACT

A series of $Li_2Fe_{1-x}V_xSiO_4/C$ ($x = 0.00$, 0.03, 0.05 and 0.07) composites have been synthesized via a refluxing-assisted solid-state reaction. XRD results confirm the monoclinic structure with space group $P2_1$ for $Li_2Fe_{1-x}V_xSiO_4/C$ compounds. TEM and Raman spectroscopy demonstrate V-doping can increase the graphitization degree of residual carbon. XPS confirms that V-incorporation does not change the divalent state of Fe, and the oxidation state of V in V-doped Li_2FeSiO_4/C is +3. Combined Ar-ion sputtering with XPS, it is found that V has been successfully doped into the crystal lattice of Li_2FeSiO_4. Electrochemical tests show that LFS/C-5 V delivers the highest initial discharge capacity of 220.4 mAh g^{-1} and the biggest Li-ion diffusion coefficient of 1.60×10^{-11} cm^2 s^{-1}. In addition, the density functional theory (DFT) calculations predict that V-doping decreases the electronic band gap of Li_2FeSiO_4, thus leads to significant improvement in the electrical conductivity of Li_2FeSiO_4. The enhanced electrochemical performance can be attributed to the increased electronic conductivity, the decreased charge transfer impedance, and the improved Li-ion diffusion coefficient. Our results clarified the nature of V doping into Li_2FeSiO_4 and demonstrated that V-doping is a promising approach to improve the electrochemical performance of Li_2FeSiO_4.

1. Introduction

With increasing global atmosphere pollution and growing exhaustion of traditional resources, people have long been involved in efficient and non-pollution energy storage materials, such as Li-air batteries [1], sodium-ion batteries [2], redox flow battery [3], Li-ion batteries [4] and so on. Among of them, Li-ion batteries attract increasing attention because of high energy density and long lifetime [4–7]. Cathode material, as one of the most important components in the lithium-ion batteries, has aroused more and more concerns [6]. The need for better large-scale batteries impels the development of new cathode materials for lithium ion batteries. Recently, a new class of polyoxyanion cathodes based on the orthosilicates, Li_2MSiO_4 (where M = Mn, Fe, and Co), has been attracting growing interest [7]. As a member of Li_2MSiO_4, Li_2FeSiO_4 (LFS) has been proposed as one of the most promising candidate for the cathode material of lithium-ion batteries due to its low cost, high safety, environmental benign, and high theoretical capacity (332 mAh g^{-1}) [7–9]. Furthermore, compared with $LiFePO_4$, LFS behaves a lower band gap and a stronger Si-O bond, which is expected to get a better cycle performance [10–14]. Unfortunately, like other polyoxyanion cathode materials (i.e., $LiFePO_4$ [4,15–17], $Li_3V_2(PO_4)_3$ [18–20], and $xLiFePO_4 \cdot yLi_3V_2(PO_4)_3$ [21,22], etc.), LFS suffers from poor capability due to its poor intrinsic electronic conductivity and slow lithium ion diffusion rate, which limits its large scale application in lithium-ion batteries. Therefore, much effort has been made to improve the electrochemical performance of LFS, such as carbon coating [9–14], particle downsizing [12,13,23,24] and metal cation doping [25–31]. Among of the above methods, metal cation doping can effectively improve the intrinsic conductivity of cathode materials, such as $LiFePO_4$ [15,16],

* Corresponding author. Tel.: +86 717 6392449; fax: +86 717 6397505.
E-mail address: xlyang@ctgu.edu.cn (X.-L. Yang).

http://dx.doi.org/10.1016/j.electacta.2014.11.172
0013-4686/

$Li_3V_2(PO_4)_3$ [20,32], and Li_2FeSiO_4 [25–30]. For instance, vanadium doping has been proved to be very effective not only for LFS [30], but also for $LiFePO_4$ [33–35], and other cathode materials [36,37]. Vanadium substitution is possible to enhance the capacity of Li_2FeSiO_4 since several oxidized vanadium states up to pentavalent (V^{5+}) are available [31]. Based on the first-principles calculations, the capacity could be enhanced by VO_4^{3-} substitution for SiO_4^{4-} in Li_2FeSiO_4 with the feasible substitution levels being less than 30% [38]. H. Hao investigated the effects of vanadium substitution at different sites (Fe/Si) on the electrochemical performance of Li_2FeSiO_4/C and found that $Li_2FeSi_{0.9}V_{0.1}O_4$/C gives the best electrochemical performance, but $Li_2Fe_{0.9}V_{0.1}SiO_4$/C exhibits poor performance [30]. However, Y. Li et al. [31] found that based on the first-principles calculations, the 50% vanadium substitution for iron in Li_2FeSiO_4 is thermodynamically more feasible, and the higher capacity may be obtained with vanadium substituted compound by exchanging more than one lithium ions. The calculated redox potentials of V^{2+}/V^{3+}, Fe^{2+}/Fe^{3+}, V^{3+}/V^{4+}, and V^{4+}/V^{5+} are 2.30, 2.87, 3.14 and 3.35 V *vs.* Li, respectively. In our previous work about $LiFePO_4$ [34], we also found appropriate vanadium substitution at Fe-site can obtain the most desirable electrochemical performance.

In this work, a series of V-doped Li_2FeSiO_4/C composites with low-level V substitution at Fe-site were prepared by a refluxing-assisted solid-state reaction. The effect of vanadium-doping on the performance of Li_2FeSiO_4 has systematically been investigated with X-ray diffraction (XRD), scanning electron microscopy (SEM), transmission electron microscopy (TEM), Raman spectroscopy, X-ray photoelectron spectroscopy (XPS), galvanostatic charge/discharge measurements, cyclic voltammetry (CV) and electrochemical impedance spectroscopy (EIS) tests. In addition, a density functional theory (DFT) calculation was also used to simulate the electronic structure to help us understand the mechanism of the improved electrochemical performance of Li_2FeSiO_4 by vanadium substitution.

2. Experimental

$Li_2Fe_{1-x}V_xSiO_4$/C (x = 0.00, 0.03, 0.05 and 0.07) composites were synthesized via a refluxing-assisted solid-state reaction. All chemicals were of analytical grade and used without further purification. A stoichiometric amount of tetraethyl orthosilicate (TEOS), $CH_3COOLi \cdot 2H_2O$, $FeC_2O_4 \cdot 2H_2O$ and V_2O_5 were dispersed in ethanol. The above mixture was refluxed at 80 °C for 24 h under stirring till a brown gel was formed. The resulting wet gel was dried at 50 °C over night. The obtained dry gel was finely ground with sucrose in acetone for 7 h. After drying, the above mixture was calcined at 350 °C for 5 h, and then sintered at 650 °C for 10 h under flowing nitrogen gas. After natural cooling down to room temperature, the powders were ground and sieved to obtain the final products. The $Li_2Fe_{1-x}V_xSiO_4$/C composites with x = 0.00, 0.03, 0.05 and 0.07 will be referred as LFS/C-0 V, LFS/C-3 V, LFS/C-5 V, LFS/C-7 V, respectively.

The phase identification of the obtained samples was performed by powder X-ray diffraction (XRD, Rigaku Ultima IV) employing Cu-kα radiation (λ = 1.5406 Å). Diffraction patterns were scanned over the range of 2θ between 10 ° and 90 °. Rietveld refinement was performed on the XRD data by using the software Maud to obtain the crystal structure parameters [21,35]. The morphology was observed with a field emission scanning electron microscopy (FESEM, JSM-7500F, JEOL) and a transmission electron microscope (TEM, JEM-2100, JEOL). Carbon coating in both samples was characterized by Raman spectrometry (LabRAM HR800, Horiba JobinYvon), and carbon content was determined by an IR carbon/sulfur determinator with high frequency induction combustion furnace (HW2000B, China). The oxidation state of key elements (Fe and V) in LFS/C-0 V and LFS/C-5 V were studied by X-ray photoelectron spectroscopy (XPS, PHI Quantera, U-P). In order to investigate the distribution of key elements (Fe, C and V) in LFS/C-0 V and LFS/C-5 V, Ar-ion sputtering was also used in XPS measurement. Electrical conductivity was measured with a standard four-probe method by RTS resistivity measurement system (RTS-8, China) on disk-shaped pellets with diameter of 8 mm and thickness of about 1.0 mm.

The electrochemical properties of the obtained samples were measured in CR2025 coin cells using lithium foil as counter and reference electrodes. The coin cells were prepared as described in Ref. 10. The working electrodes were prepared by mixing active materials (75 wt.%), acetylene black (15 wt.%) and polyvinylidene fluoride (PVDF, 10 wt.%) in N-methyl pyrrolidinone (0.02 g mL^{-1}) on an aluminum foil (20 μm in thickness) which was used as the current collectors. The loading of the active materials on the electrode was about 1.8 mg cm^{-2}. Galvanostatic charge-discharge measurements were performed in a voltage range of 1.5–4.8 V on a battery test system (LAND CT2001A, China). All reported capacities are quoted with respect to the mass of the obtained samples including the carbon. Cyclic voltammetry (CV) and electrochemical impedance spectroscopy (EIS) measurement were performed on an electrochemical working station (CHI614C, China). CV curves were monitored at a slow scanning rate of 0.05 mV s^{-1} within a voltage range of 1.5–4.8 V; EIS spectra were obtained over a frequency range from 0.01 Hz to 100 kHz.

3. Results and discussion

Fig. 1 shows the XRD patterns of the prepared $Li_2Fe_{1-x}V_xSiO_4$/C (x = 0.00, 0.03, 0.05 and 0.07) composites. In spite of some impurities, such as Li_2SiO_3, $Fe_{2.936}O_4$, and Fe_7SiO_{10}, appeared in the XRD patterns due to volatilization of stoichiometric Li, the main diffraction peaks of the four samples are well indexed to a monoclinic structure phase (JCPDS No. 77-4374) with a space group of $P2_1$, which indicates that V-incorporation has no inherent effect on the lattice structure of Li_2FeSiO_4. A full Rietveld refinement was carried out on LFS/C-0 V and LFS/C-5 V, and the results are shown in Fig. 2, Table 1 and Table 2. The best refinement model was chosen from a $P2_1/n$ space group, and satisfactory and acceptable reliability factor (S<2) is obtained. It can be clearly seen that, after V-doping, the unit cell volume decreases, which could be explained by the substitution of V^{3+} (the

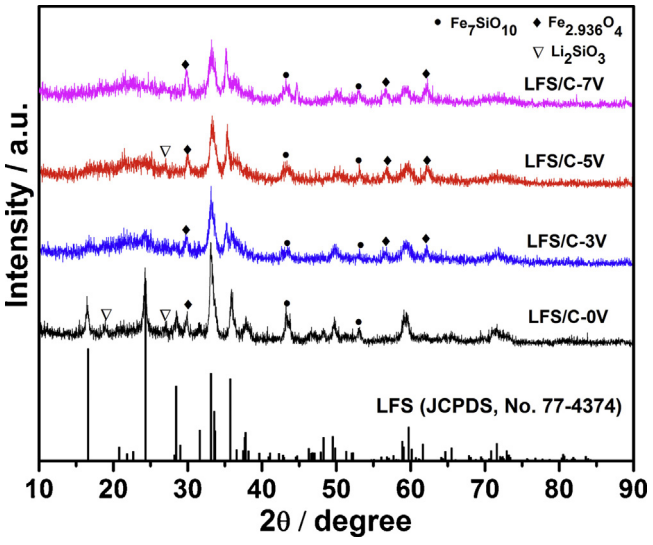

Fig. 1. XRD patterns of LFS/C-0 V, LFS/C-3 V, LFS/C-5 V, and LFS/C-7 V samples.

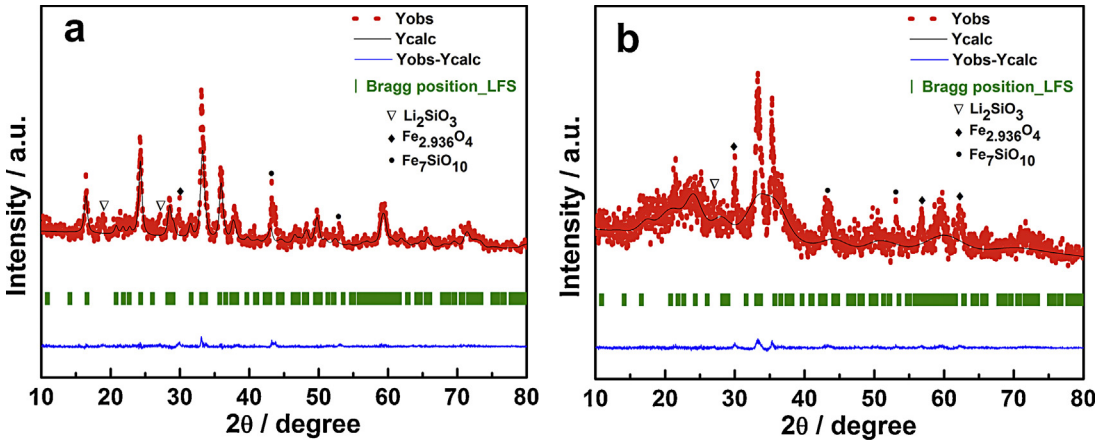

Fig. 2. XRD Rietveld refinement results of (a)LFS/C-0 V, and (b)LFS/C-5 V.

Table 1
Lattice parameters of LFS/C-0 V and LFS/C-5 V.

Sample	*a* (Å)	*b* (Å)	*c* (Å)	*V* (Å^3)	*S*
LFS/C-0V	8.2586	4.9939	8.2286	339.37	1.25
LFS/C-5V	8.3298	5.0266	7.9809	334.16	1.27

Table 2
Atomic fractional coordinates of LFS/C-0 V and LFS/C-5 V.

Atom		*x*	*y*	*z*
LFS/C-0V	Li_1	0.6799	0.8902	0.6697
	Li_2	0.5947	0.2877	0.0589
	Fe_1	0.2831	0.8101	0.5474
	Si_1	0.0305	0.8157	0.7939
	O_1	0.8872	0.7970	0.8430
	O_2	0.3980	0.2030	0.8987
	O_3	0.6877	0.7615	0.4798
	O_4	0.9802	0.8128	0.2309
LFS/C-5V	Li_1	0.6204	0.7431	0.6629
	Li_2	0.5926	0.3683	0.0371
	$Fe_1(V_1)$	0.2807	0.8109	0.5492
	Si_1	0.0283	0.8049	0.7543
	O_1	0.8718	0.6652	0.8660
	O_2	0.3945	0.2371	0.9714
	O_3	0.6994	0.7530	0.4343
	O_4	0.9682	0.8142	0.2183

radius is 0.074 nm) for Fe^{2+} (the radius is 0.076 nm) [30]. To further verify V-doping into the LFS lattice, XPS measurements were carried out, as discussed later. Moreover, there is no evidence of crystalline carbon diffraction peaks for the four samples, which indicates that residual carbon is in amorphous form. The carbon content in LFS/C, LFS/C-3 V, LFS/C-5 V and LFS/C-7 V is measured to be 8.84, 8.60, 8.04 and 7.51 wt.%, respectively (Table 3). It is found that the carbon content decreases with the increase of the vanadium content, because the pyrolytic carbon was increasingly consumed for the reduction of V^{5+} to V^{3+} during the synthesis process [34].

Table 3
The electronic conductivity and carbon content of samples.

Sample	Carbon content (wt.%)	Electronic conductivity (S cm^{-1})
LFS/C-0V	8.84	2.50×10^{-4}
LFS/C-3V	8.60	3.66×10^{-4}
LFS/C-5V	8.04	3.07×10^{-4}
LFS/C-7V	7.51	2.61×10^{-4}

The SEM images of samples in Fig. 3 shows that LFS/C with V-incorporation exhibits less agglomeration, especially when *x* is 0.05. The microstructure of LFS/C-0 V and LFS/C-5 V is further observed using TEM. As seen in Fig. 4, both samples are composed of many nanocrystals of LFS with a size of 50–100 nm, especially some smaller nanoparticles (7–10 nm) are also detected in the LFS/C-5 V sample (Fig. 4d). LFS particles in both samples are embedded in carbon network or connected/coated tightly by carbon, which may inhibit grain growth and enhance the electronic conductivity of the material. Figs. 4b and d show clear lattice fringes with d-spacing of 0.2364, 0.2504 and 0.2640 nm, which corresponds to the (212), (020) and (-212) planes of monoclinic LFS, respectively, which indicates that LFS is very crystalline. Noting that, graphite is easier to be detected in the LFS/C-5 V sample, which demonstrates V-doping is favorable for increasing the graphitization degree of residual carbon [34].

Raman spectroscopy was performed to further study the structural property of residual carbon in LFS/C-0 V and LFS/C-5 V. From Fig. 5, it can be clearly seen that two broad peaks appear at ~1350 and ~1600 cm^{-1}, which correspond to the D (sp^3-type) and G (sp^2-type) bands of the residual carbon in both samples, respectively [39]. The intensity ratio of D and G bands is usually used to evaluate the graphitization degree of carbon. The lower I_D/I_G ratio, the higher the graphitization degree of the residual carbon is. Obviously, LFS/C-5 V shows a much lower I_D/I_G ratio of 0.63 than LFS/C-0 V (1.85), which demonstrates that V-doping can improve the graphitization degree of the residual carbon. This result is in good agreement with TEM results and our previous reports [34]. Moreover, higher graphitization degree of the residual carbon in LFS/C-5 V means higher electronic conductivity for LFS/C-5 V sample, which is verified by the measured electronic conductivity (3.07×10^{-4} S cm^{-1} for LFS/C-5 V, but 2.50×10^{-4} S cm^{-1} for LFS/C-0 V).

X-ray photoelectron spectroscopy (XPS) is a useful tool to study the oxidation state of key elements in samples, and also an important surface analysis technique to investigate the element distribution [20,26]. Fig. 6 is the XPS spectra of LFS/C-0 V and LFS/C-5 V. The binding energy (BE) scales were calibrated by carbon (C1s = 284.5 eV). From Fig. 6a_2 and b_2, it can be clearly seen that the Fe2$p_{3/2}$ main peak at ~710 eV is very close to that for the Fe^{2+} in $LiFePO_4$ [40], which indicate that V-incorporation does not change the divalent state of Fe in LFS. As shown in Fig. 6b_4, the V2$p_{3/2}$ main peak at ~516.6 eV is consistent with that of V^{3+} in $Li_3V_2(PO_4)_3$ [41], confirming that the oxidation state of V in LFS/C-5 V is +3. Furthermore, the intensity of C1s on the surface of both samples is much stronger

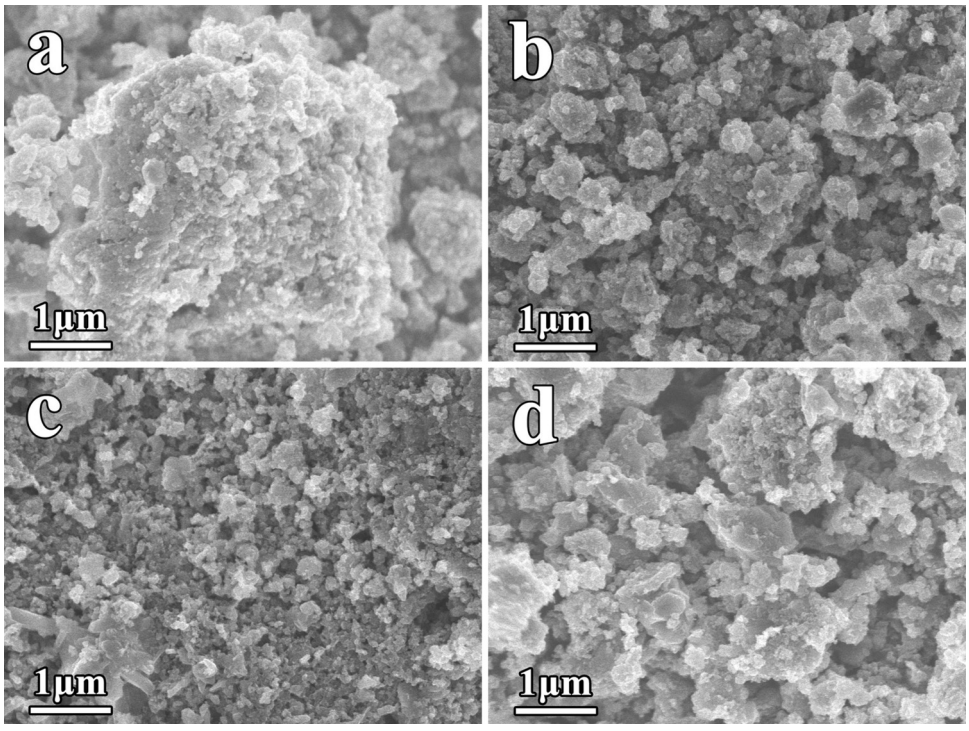

Fig. 3. SEM images of (a)LFS/C-0 V, (b)LFS/C-3 V, (c)LFS/C-5 V, and (d)LFS/C-7 V.

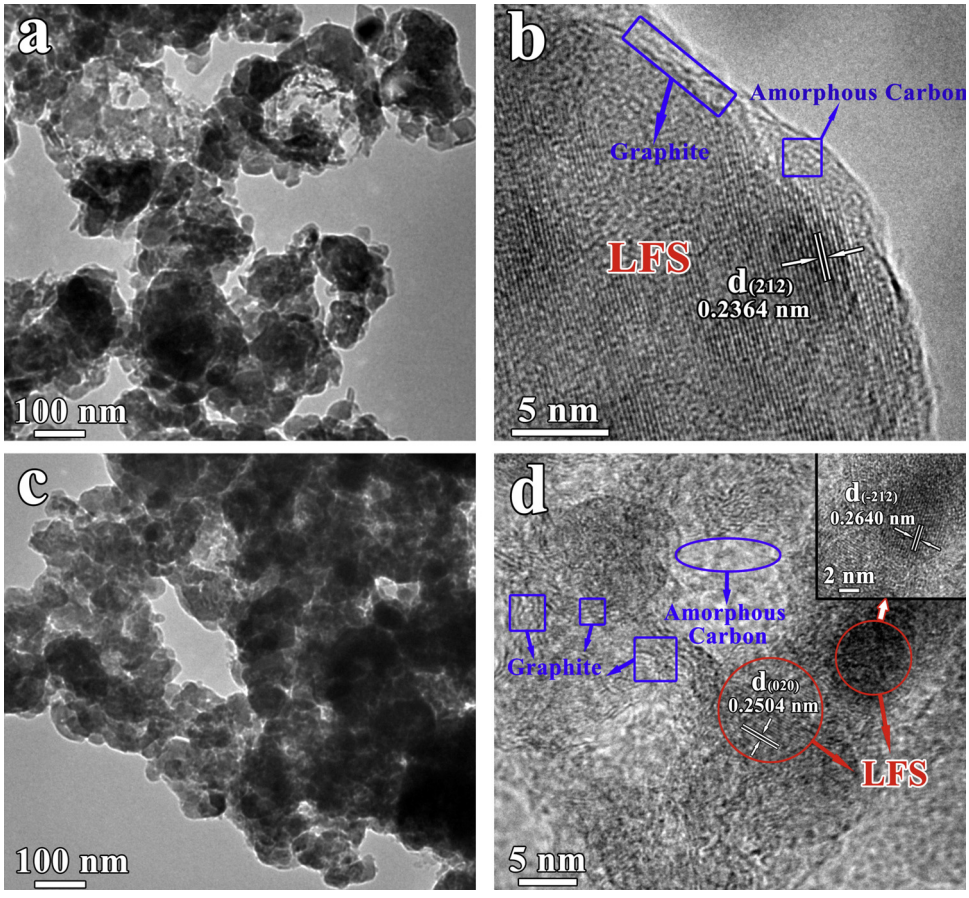

Fig. 4. TEM images of (a,b)LFS/C-0 V, and (c,d)LFS/C-5 V.

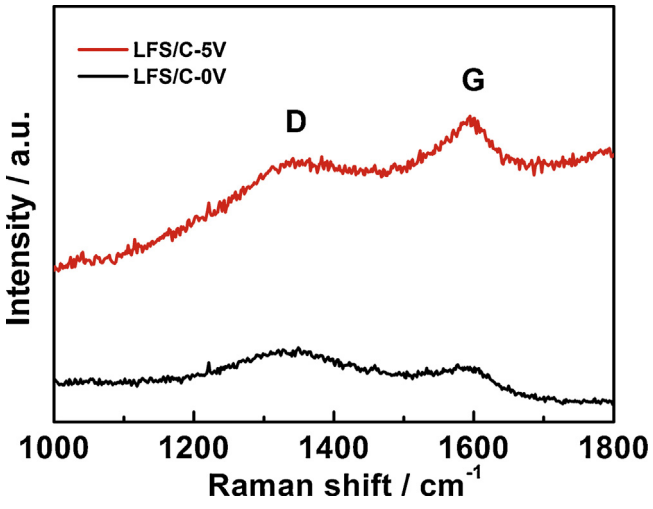

Fig. 5. The Raman spectra of LFS/C-0 V and LFS/C-5 V.

than that in the interior (Fig. 6a_3 and b_3), which reveals that carbon is just coated on the surface of both samples. Instead, the intensity of Fe2$p_{3/2}$ main peaks (Fig. 6a_2 and b_2) on the surface is much lower than that in the interior due to the carbon coating layer. Noting that, as shown in Fig. 6b_4, V2$p_{3/2}$ spectrum exhibits stronger peaks in the interior but weaker on the surface. Therefore, it is reasonable to believe that, in addition to a trifle of V exists on the surface in a form of V-containing composites, a majority of V enters into the lattice of LFS. For all we know, V^{3+} is easier to form VO_4 tetrahedra, thus V^{3+} would be doped at the Fe-site in the LFS lattice. Considering the stability of SiO_4 tetrahedra, it is difficult to form an oxygen vacancy; instead, $Li_{2-x}Fe^{2+}{}_{1-y}V^{3+}{}_ySiO_4$ would be formed to keep the charge balance, indicative of the presence of vacancies in the Li crystallographic sites, which can provide a much enhanced ionic conductivity, and thus an improved electrochemical performance of LFS [42].

Fig. 7 shows the first two charge/discharge profiles and cycle performance curves of $Li_2Fe_{1-x}V_xSiO_4$/C samples at 0.1 C and 1 C within the potential range of 1.5–4.8 V. As seen in Fig. 7a_1 and b_1, two potential plateaus located at ~2.8 V and ~4.6 V, corresponding to the Fe^{2+}/Fe^{3+} and Fe^{3+}/Fe^{4+} redox couples, respectively, can be observed in the initial charge curves for the four samples, which agrees well with previous reports [10,43]. As can be clearly seen in Table 4, LFS/C-5 V delivers the highest initial discharge capacity of 220.4 mAh g^{-1}, corresponding to 1.33 mol Li^+, which suggests that more than one Li^+ can be extracted from LFS. After 50 cycles at 0.1 C, LFS/C-5 V also exhibits the highest discharge capacity of 146.6 mAh g^{-1} with the highest capacity retention ratio of 78.7%, which is higher than LFS/C-0 V (77.7 mAh g^{-1}, 59.6%). Here, it should be noted that, considering that penetration of electrolyte into the electrode, structural change, and solid electrolyte interphase (SEI) formation of electrode can be completed in the second cycle, we choose the second cycle to calculate the capacity retention ratio. Even after 50 cycles at a higher rate as 1 C, all the V-doped LFS/C samples show enhanced discharge capacities. For instance, the LFS/C-5 V electrode delivers the highest capacity of 112.1 mAh g^{-1}, while LFS/C-0 V only shows a capacity of 92.0 mAh g^{-1}. In a word, V-doping can significantly improve the electrochemical performance of LFS.

To understand the electrochemical behavior of the pristine and V-doped LFS/C samples, CV tests were conducted at a slow scanning rate of 0.05 mV s^{-1}. From Fig. 8, it is apparent that the CV curves of LFS/C-0 V and LFS/C-5 V are very similar. Two anodic peaks occur at ~3.15 V and ~4.8 V during the first charging process. The anodic peak at ~3.15 V corresponds to the oxidation of Fe^{2+}/Fe^{3+}. Noting that, during the subsequent charging process, the anodic peaks associated with the oxidation of Fe^{2+}/Fe^{3+} shift to a lower potential (~2.95 V), indicative of a structural rearrangement [44,45]. The anodic peak at ~4.8 V might be ascribed to the decomposition of electrolyte. Interestingly, an extra cathodic peak at ~1.8 V is also observed, which should be ascribed to the reaction of forming the solid electrolyte interface (SEI) film on the positive electrode surface [46] or to some extra side reaction [47]. As we all know, the small the difference between reduction and oxidation potentials for electrode materials, the better the reversibility of electrode reaction is. It can be clearly seen in Table 6, LFS/C-5 V shows smaller potential difference, indicative of better reversibility.

To the best of our knowledge, preliminary information on electron conductivity can be obtained from the DOS of composites [31], so density functional theory (DFT) calculations were performed to examine the effect of V-substitution on the electron conductivity of LFS. From Fig. 9, it can be clearly seen that isolate states (come from V) appears in the covalence band and Fermi level upshifts. Moreover, the electronic band gap of $Li_2Fe_{0.94}V_{0.06}SiO_4$ is 1.8 eV, which is less than half of Li_2FeSiO_4 (3.7 eV). Obviously, V-substitution can improve the electronic conductivity of LFS, which is in agreement with the measured results listed in Table 3. For instance, the LFS/C-0 V shows the lowest electronic conductivity. Nevertheless, with the increase of vanadium content, the electronic conductivity is not a linear increase. At a low-level doping (LFS/C-3 V), the carbon content is slightly reduced, so its improved electronic conductivity mainly results from the decreased electronic band gap of LFS and the increased graphitization degree of residual carbon. With the continuous increase of vanadium content (i.e., LFS/C-5 V and LFS/C-7 V), carbon content is highly reduced because of the increasing consumption of pyrolytic carbon, leading to a linear decrease in electronic conductivity.

The electrochemical impedance spectroscopies (EIS) for the $Li_2Fe_{1-x}V_xSiO_4$/C samples are shown in Fig. 10. All EIS spectra are composed of a small intercept in the highest frequency region, a depressed semicircle at the medium frequency region, combing with an inclined line in the low-frequency region. The small intercept corresponds to the ohmic resistance, representing the resistance of the electrolyte. The depressed semicircle is attributed to the charge transfer resistance and the double-layer capacitance between the electrolyte and cathode. The inclined line is related to the Warburg impedance, which is associated with Li^+ ion diffusion in the cathode active particles [14]. All EIS curves were fitted by an equivalent circuit composed of "R(C(RW))" using the ZSimpWin program, and the fitting results were shown Table 5. The smaller the diameter, the lower the charge-transfer resistance is. From Fig. 10a and Table 5, it is found that LFS/C-5 V shows the lowest charge-transfer resistance (R_{ct} = 26.19 Ω). The diffusion coefficient of lithium ions (D_{Li}) can be obtained according to the following equations [11,14]:

$$D_{Li} = R^2T^2/2A^2n^2F^4C_{Li}^2\delta^2 \quad (1)$$

Where R is the gas constant, T is the absolute temperature, A is the surface area of the cathode, n is the number of electrons per molecule during oxidation, F is the Faraday constant, C_{Li} is the concentration of lithium ion. δ *is* the Warburg coefficient which is related to Z' [11,14]:

$$Z' = R_c + R_{ct} + \delta\omega^{-1/2} \quad (2)$$

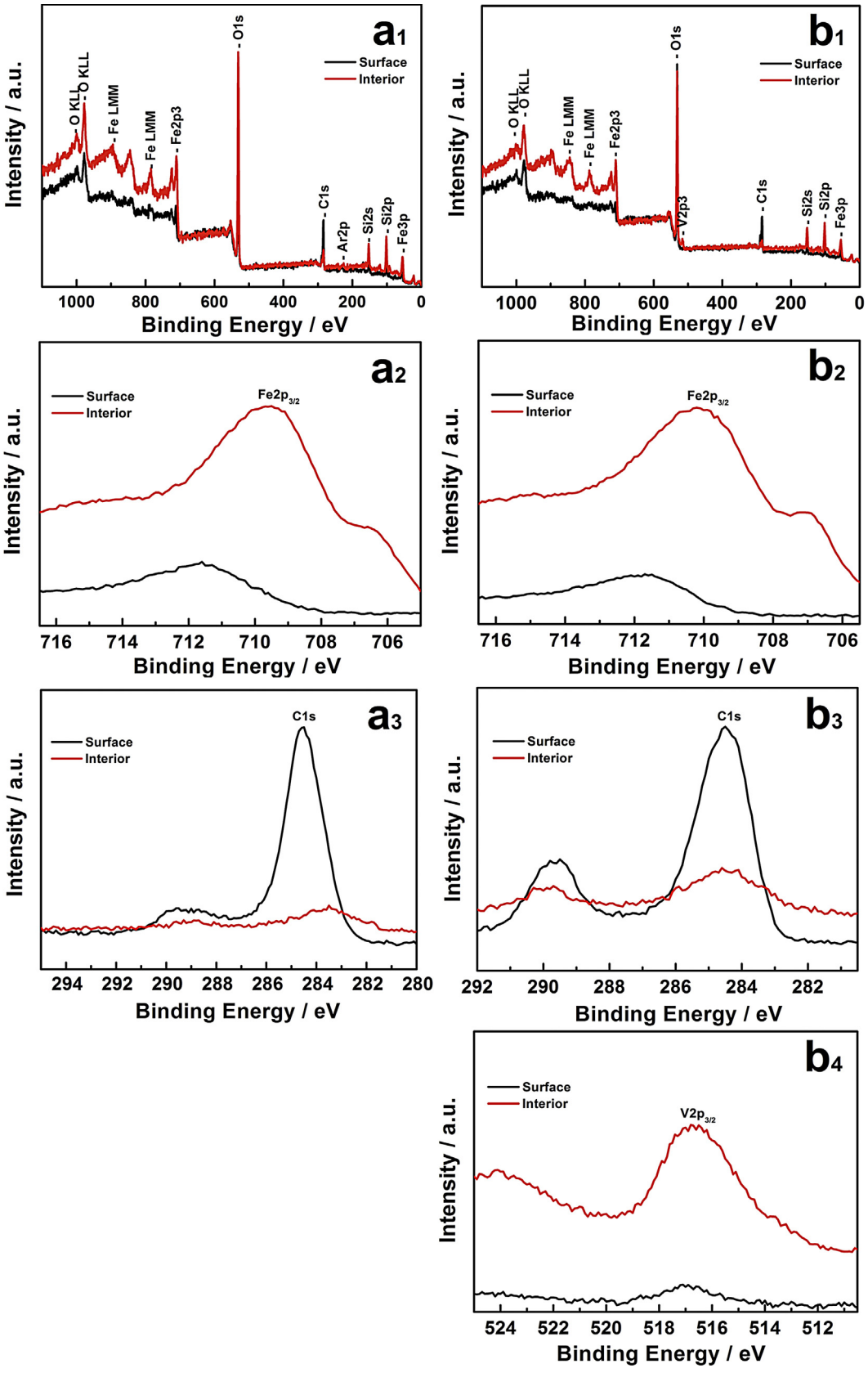

Fig. 6. XPS spectra of (a)LFS/C-0 V, and (b)LFS/C-5 V.

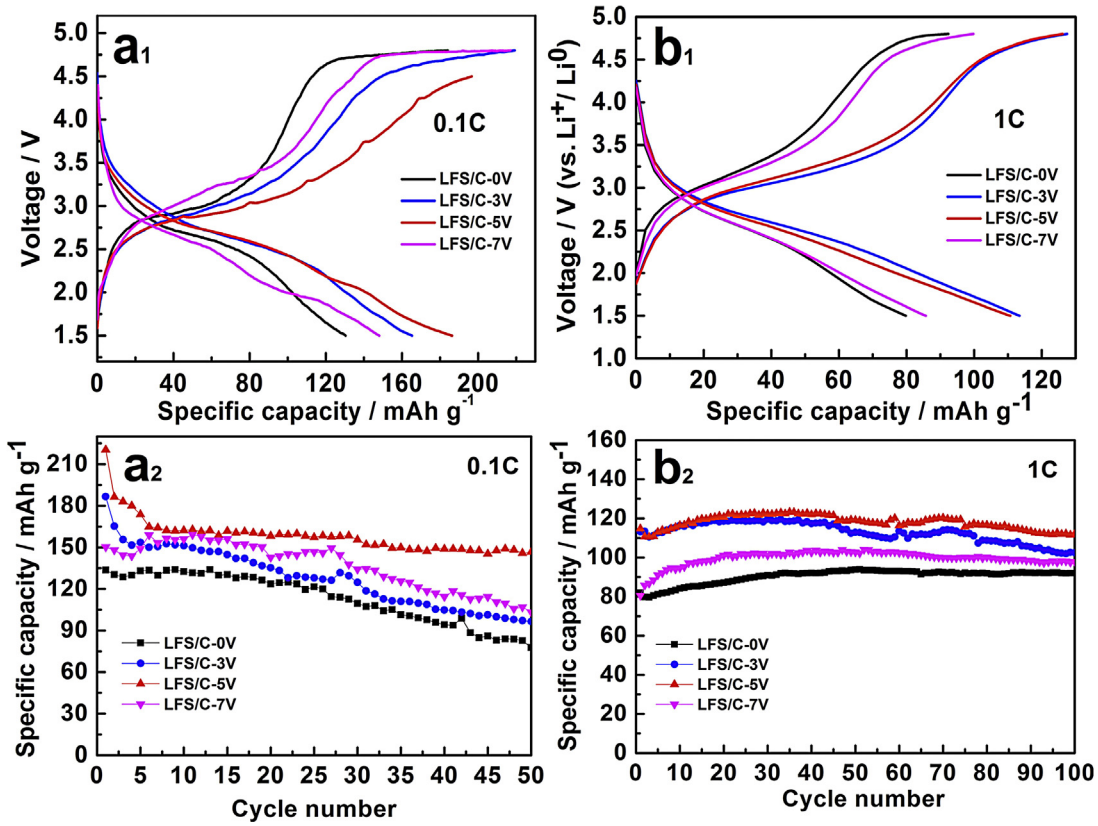

Fig. 7. The second charge/discharge profiles and cycle performance curves of LFS/C-0 V, LFS/C-3 V, LFS/C-5 V, and LFS/C-7 V samples at 0.1 C and 1 C.

Table 4
Discharge capacity of the 1st, 2nd and 50th cycles at 0.1 C of the samples.

	LFS/C-0V	LFS/C-3V	LFS/C-5V	LFS/C-7V
1st (mAh g^{-1})	133.7	186.6	220.4	150.3
2nd (mAh g^{-1})	130.4	165.3	186.3	148.1
50th (mAh g^{-1})	77.7	96.5	146.6	103.2
Capacity retention ratio* (%)	59.6	58.4	78.7	69.7

* Capacity retention ratio compared to the second cycle.

Table 5
EIS Parameters of samples.

Sample	R_{ct} (Ω)	δ (Ω $s^{-1/2}$)	D_{Li} (cm^2 s^{-1})
LFS/C-0V	47.26	38.17	1.03×10^{-11}
LFS/C-3V	30.52	32.95	1.38×10^{-11}
LFS/C-5V	26.19	30.65	1.60×10^{-11}
LFS/C-7V	45.16	42.65	0.82×10^{-11}

Where ω is the angular frequency in the low frequency region, both R_C and R_{ct} are kinetics parameters independent of frequency, so δ is also the slope for the plot of Z' *vs.* the reciprocal square root of the lower angular frequencies ($\omega^{-1/2}$). To obtain the Warburg coefficient (δ), the linear fitting of Z' *vs.* $\omega^{-1/2}$ in the low frequency region of $Li_2Fe_{1-x}V_xSiO_4/C$ ($x = 0.00$, 0.03, 0.05 and 0.07) samples is shown in Fig. 10b. As listed in Table 5, LFS/C-5 V shows the highest increased diffusion coefficient of lithium ions ($D_{Li} = 1.60 \times 10^{-11}$ cm^2 s^{-1}) than LFS/C-0 V ($D_{Li} = 1.03 \times 10^{-11}$ cm^2 s^{-1}) and other V-doped samples (For LFS/C-3 V, $D_{Li} = 1.38 \times 10^{-11}$ cm^2 s^{-1}; and for LFS/C-7 V, $D_{Li} = 0.82 \times 10^{-11}$ cm^2 s^{-1}), which confirms that LFS/C-5 V presents the fastest kinetics of the cell reactions. The EIS results also agree well with the results of electrochemical performance tests.

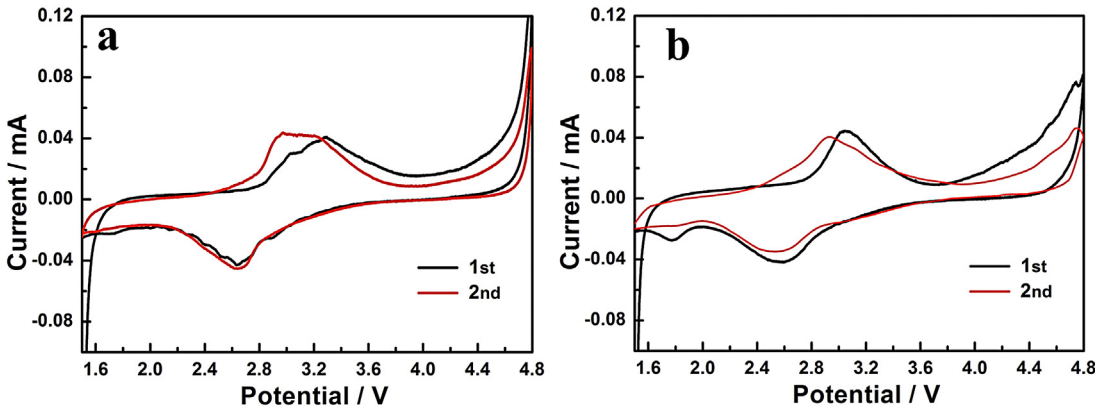

Fig. 8. CV profiles of (a)LFS/C-0 V, and (b)LFS/C-5 V.

Table 6
The peak potential of LFS/C-0 V and LFS/C-5 V

	LFS/C-0V		LFS/C-5V	
	1st	2nd	1st	2nd
E_A (V)	3.286	3.090	3.043	2.937
E_C (V)	2.632	2.634	2.569	2.536
$\Delta E_{A\text{-}C}$ (V)	0.654	0.456	0.474	0.401

be attributed to the increased electronic conductivity, the decreased charge transfer impedance, and the improved Li-ion diffusion coefficient. We believe that V-doping may be a promising method to improve the electrochemical performance of other cathode materials suffering from inferior electronic conductivity.

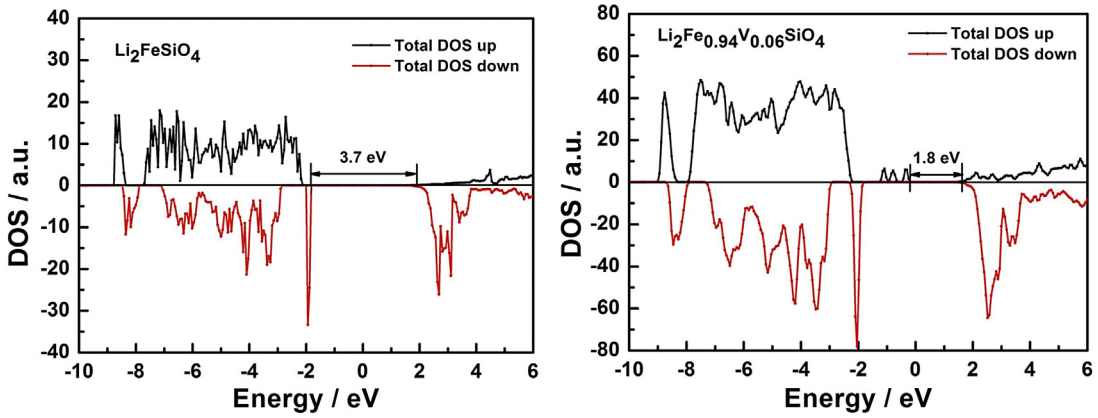

Fig. 9. Calculated density of state (DOS) patterns of Li_2FeSiO_4 and $Li_2Fe_{0.94}V_{0.06}SiO_4$.

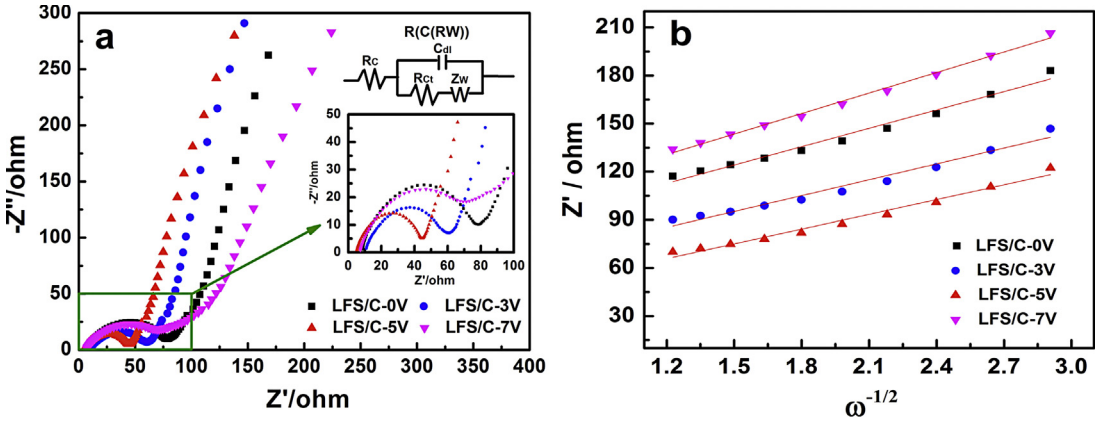

Fig. 10. (a) EIS curves, and (b) relationship between Z′ and $\omega^{-1/2}$ in the low frequency region of LFS/C-0 V, LFS/C-3 V, LFS/C-5 V, and LFS/C-7 V samples.

4. Conclusions

V-doped Li_2FeSiO_4/C composites with monoclinic structure were successfully synthesized via a refluxing-assisted solid-state reaction. TEM and Raman spectroscopy demonstrate V-doping can increase the graphitization degree of residual carbon. XPS verifies that V-incorporation does not change the divalent state of Fe, and the oxidation state of V in V-doped Li_2FeSiO_4/C is +3; moreover, V has been successfully doped into the crystal lattice of Li_2FeSiO_4. Compared with the pristine Li_2FeSiO_4/C, V-doped Li_2FeSiO_4/C composites present better electrochemical performance, especially $Li_2Fe_{0.95}V_{0.05}SiO_4$/C delivers the highest initial discharge capacity of 220.4 mAh g^{-1} and the biggest Li-ion diffusion coefficient of 1.60×10^{-11} cm^2 s^{-1}. By combining the density functional theory calculations, we have demonstrated that V-doping is a promising approach to significantly enhance the electrchemical performance of Li_2FeSiO_4 cathodes. The improved electrochemical performance can

Acknowledgments

This work was supported by the National Science Foundation of China(51302153, 51272128); the Key Project of Hubei Provincial Department of Education (D20131303); the Opening Project of CAS Key Laboratory of Materials for Energy Conversion (CKEM131404); the Scientific Fund of China Three Gorges University (KJ2012B043); the Research Innovation Foundation of Master Dissertation of China Three Gorges University (2013CX028); and the Faculty Research Grant (FRG) from Sam Houston State University.

References

[1] L. Li, S.H. Chai, S. Dai, A. Manthiram, Energy Environ. Sci. 7 (2014) 2630.
[2] W. Luo, J. Schardt, C. Bommier, B. Wang, J. Razink, J. Simonsen, X. Ji, J. Mater. Chem. A 1 (2013) 10662.
[3] W. Wang, Q. Luo, B. Li, X. Wei, L. Li, Z. Yang, Adv. Funct. Mater. 23 (2013) 970.

[4] A.K. Padhi, K.S. Nanjundaswamy, J.B. Goodenough, J. Electrochem. Soc. 144 (1997) 1188.
[5] T. Kodama, H. Sakaebe, J. Power Sources 81–82 (1999) 144.
[6] B. Xu, D. Qian, Z. Wang, Y.S. Meng, Mater. Sci. Eng. R 73 (2012) 51.
[7] M.S. Islam, R. Dominko, C. Masquelier, C. Sirisopanaporn, A.R. Armstrong, P.G. Bruce, J. Mater. Chem. 27 (2011) 9811.
[8] A.R. Armstrong, N. Kuganathan, M.S. Islam, P.G. Bruce, J. Am. Chem. Soc. 133 (2011) 13031.
[9] A. Nytén, A. Abouimrane, M. Armand, T. Gustafsson, J.O. Thomas, Electrochem. Commun. 7 (2005) 156.
[10] H. Zhu, X. Wu, L. Zan, Y. Zhang, Electrochim. Acta 117 (2014) 34.
[11] G. Peng, L.L. Zhang, X.L. Yang, S. Duan, G. Liang, Y.H. Huang, J. Alloys Compd. 570 (2013) 1.
[12] Z.L. Gong, Y.X. Li, G.N. He, J. Li, Y. Yang, Electrochem. Solid-State Lett. 11 (2008) A60.
[13] H. Zhou, M.A. Einarsrud, F. Vullum-Bruer, J. Power Sources 235 (2013) 234.
[14] L.L. Zhang, S. Duan, X.L. Yang, G. Peng, G. Liang, Y.H. Huang, Y. Jiang, S.B. Ni, M. Li, ACS Appl. Mater. Interfaces 5 (2013) 12304.
[15] L.X. Yuan, Z.H. Wang, W.X. Zhang, X.L. Hu, J.T. Chen, Y.H. Huang, J.B. Goodenough, Energ. Environ. Sci. 4 (2011) 269.
[16] S.Y. Chung, Y.M. Chiang, Electrochem. Solid-State Lett. 6 (2003) A278.
[17] G. Qin, Q. Ma, C. Wang, Electrochim. Acta 115 (2014) 407.
[18] H. Huang, S.C. Yin, T. Kerr, N. Taylor, L.F. Nazar, Adv. Mater. 14 (2002) 1525.
[19] Y.Q. Qiao, J.P. Tu, X.L. Wang, D. Zhang, J.Y. Xiang, Y.J. Mai, C.D. Gu, J. Power Sources 196 (2011) 7715.
[20] L.L. Zhang, G. Liang, G. Peng, Y.H. Huang, L. Wang, L. Qie, M.C. Croft, A. Ignatov, J. B. Goodenough, J. Electrochem. Soc. 159 (2012) A1573.
[21] S. Zhong, L. Wu, J. Liu, Electrochim. Acta 74 (2012) 8.
[22] L. Wu, J. Lu, G. Wei, P. Wang, H. Ding, J. Zheng, X. Li, S. Zhong, Electrochim. Acta 146 (2014) 288.
[23] Z. Zheng, Y. Wang, A. Zhang, T. Zhang, F. Cheng, Z. Tao, J. Chen, J. Power Sources 198 (2012) 229.
[24] J. Cui, C. Qing, Q. Zhang, C. Su, X. Wang, B. Yang, X. Huang, Ionics 20 (2014) 23.
[25] R. Chen, R. Heinzmann, S. Mangold, V.S.K. Chakravadhanula, H. Hahn, S. Indris, J. Phys. Chem. C 117 (2013) 884.
[26] H. Guo, X. Cao, X. Li, L. Li, X. Li, Z. Wang, W. Peng, Q. Li, Electrochim. Acta 55 (2010) 8036.
[27] S. Zhang, C. Deng, B.L. Fu, S.Y. Yang, L. Ma, Electrochim. Acta 55 (2010) 8482.
[28] L.L. Zhang, S. Duan, X.L. Yang, G. Liang, Y.H. Huang, X.Z. Cao, J. Yang, S.B. Ni, M. Li, Scientific Reports 4 (2014) 5064.
[29] C. Deng, S. Zhang, S.Y. Yang, B.L. Fu, L. Ma, J. Power Sources 196 (2011) 386.
[30] H. Hao, J. Wang, J. Liu, T. Huang, A. Yu, J. Power Sources 210 (2012) 397.
[31] Y. Li, X. Cheng, Y. Zhang, J. Electrochem. Soc. 159 (2012) A69.
[32] Y.Z. Dong, Y.M. Zhao, H. Duan, J. Electroanal. Chem. 660 (2011) 14.
[33] F. Omenya, N.A. Chernova, S. Upreti, P.Y. Zavalij, K.W. Nam, X.Q. Yang, M.S. Whittingham, Chem. Mater. 23 (2011) 4733.
[34] L.L. Zhang, G. Liang, A. Ignatov, M.C. Croft, X.Q. Xiong, I.M. Hung, Y.H. Huang, X. L. Hu, W.X. Zhang, Y.L. Peng, J. Phys. Chem. C 115 (2011) 13520.
[35] J. Ma, B. Li, H. Du, C. Xu, F. Kang, J. Electrochem. Soc. 158 (2011) A26.
[36] F. Wang, J. Yang, Y. NuLi, J. Wang, J. Power Sources 195 (2010) 6884.
[37] N. Jayaprakash, N. Kalaiselvi, Gangulibabu, D. Bhuvaneswari, J. Solid State Electrochem. 15 (2011) 1243.
[38] A. Liivat, J.O. Thomas, Comput. Mater. Sci. 50 (2010) 191.
[39] M.M. Doeff, Y.Q. Hu, F. McLarnon, R. Kostecki, Electrochem. Solid-State Lett. 6 (2003) A207.
[40] C.S. Sun, Z. Zhou, Z.G. Xu, D.G. Wang, J.P. Wei, X.K. Bian, J. Yan, J. Power Sources 193 (2009) 841.
[41] H. Liu, C. Cheng, X. Huang, J. Li, Electrochim. Acta 55 (2010) 8461.
[42] X. Huang, H. Chen, H. Wang, S. Zhou, Y. Chen, B. Liu, J. Yang, G. Zhou, Q. Jiang, M. Qu, Z. Pan, Z. Yu, Solid State Ionics 220 (2012) 18.
[43] D. Lv, W. Wen, X. Huang, J. Bai, J. Mi, S. Wu, Y. Yang, J. Mater. Chem. 21 (2011) 9506.
[44] A. Nytén, S. Kamali, L. Häggström, T. Gustafsson, J.O. Thomas, J. Mater. Chem. 16 (2006) 2266.
[45] P. Zhang, Y. Zheng, S. Yu, S.Q. Wu, Y.H. Wen, Z.Z. Zhu, Y. Yang, Electrochim. Acta 111 (2013) 172.
[46] C.Y. Hu, J. Guo, S.J. Li, Y.X. Peng, J. Wen, J. Cent. South Univ. 19 (2012) 1791.
[47] S. Singh, S. Mitra, Electrochim. Acta 123 (2014) 378.